ResearchGate

See discussions, stats, and author profiles for this publication at: https://www.researchgate.net/publication/359383830

Sub-50 nm control of light at 405 nm with planar Si nanolens

Article *in* Optics Express · March 2022

CITATIONS
0

READS
2

3 authors, including:

Zhong Wang
Nanjing University
1 PUBLICATION 0 CITATIONS
SEE PROFILE

Weihua Zhang
Nanjing University
81 PUBLICATIONS 2,898 CITATIONS
SEE PROFILE

Some of the authors of this publication are also working on these related projects:

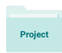
Sub-50 nm control of light at 405 nm with planar Si nanolens View project

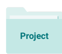
Plasmonics applications View project

All content following this page was uploaded by Zhong Wang on 21 March 2022.

The user has requested enhancement of the downloaded file.

Sub-50 nm control of light at 405 nm with planar Si nanolens

ZHONG WANG, MULING CHEN AND WEIHUA ZHANG*

College of Engineering and Applied Sciences, Jiangsu Key Laboratory of Artificial Functional Materials, MOE Key Laboratory of Intelligent Optical Sensing and Manipulation, State Key Laboratory of Analytical Chemistry for Life Sciences, Nanjing University, Nanjing 210093, China

** zwh@nju.edu.cn*

Abstract: We studied the super-resolution light modulation capability of Si nanodisks, a flat semi-transparent high index nanolens in the visible spectral range. A Laguerre-Gaussian beam-based optimization algorithm was developed to synthesize desired field distributions. Focused spots below 45 nm ($< \lambda/9$) were successfully achieved with 405 nm light over the whole center area of the nanolens. This superb light nano-focusing capability allows us to synthesize complex nano-patterns by simply superposing several focus spots together, making the Si nanolens a promising tool for super-resolution photolithography.

© 2022 Optical Society of America under the terms of the OSA Open Access Publishing Agreement

1. Introduction

The optical resolution can be improved by using high refractive index materials. This method has been widely used with liquid, for instance oil immersion objective lenses [1-3] and water-immersion Deep Ultraviolet (DUV) lithography [4-6]. Recently, it was extended to solid dielectric materials, particularly micro-dielectric structures, such as polymer micro-droplets [7], dielectric microspheres [8] and TiO2 nanoparticle micro-droplets [9]. A variety of interesting results have been reported, such as super-resolution white-light imaging [8, 10-15], fluorescence imaging [16-19], and lithography [20-22], to name a few. Despite the successes, the resolution of dielectric micro-lenses is fundamentally limited by their refractive index, which is normally lower than 2.0 in the visible spectral range. As a result, the smallest resolvable pitch size is limited to a value slightly better than 100 nm. Moreover, these micro-dielectric lenses are normally curved 3-dimensional structures, which cannot be produced using standard nano-fabrication techniques. Herein, we ask the following questions: "(1) Can we make a high index lens which can modulate light with spatial resolution well below 100 nm, and (2) can this lens be a flat structure which can be easily fabricated?"

To answer the above questions, we investigate the optical behaviors of a simple flat high index nanostructure, Si nanodisk, and study whether we can focus, scan and even generate any given pattern of light at the nanoscale using such a structure. Here, Si is chosen because high index materials commonly have a narrow bandgap which is associated with high material losses in the visible range but Si is an exception [23, 24]. As an indirect band material, the absorption of Si is considerably lower than those of direct band materials in the visible and near-infrared spectral range. For example, the penetration depth of Si is approximately 200 nm at 405 nm, one of the most commonly used wavelengths for photolithography [25]. This is enough for building a Si nano-lens with a reasonable transmissivity. For example, we demonstrated that sub-50 nm focus can be achieved with a simple semispherical nanolens, but as a 3D structure, it is extremely difficult to fabricate [26].

To check whether the flat Si lens can focus and further spatially modulate light at will, we need to solve an inverse problem. That is, for a target super-resolution field distribution, whether we can find corresponding incident fields, and what they are. Today, driven by the fast development of computational electrodynamics, this type of inverse problems have been attracting a lot of interests [27-31], and different algorithms were developed in various

47 scenarios, for instance three-dimensional vectorial holography [29], surface plasmon [28], and
48 Au nanostructure arrays [32]. In this work, we use a high-order Laguerre-Gaussian (LG) beam
49 [33-35] based method together with a customized particle swarm optimization (PSO) algorithm
50 [36, 37] to solve the inverse problem.

51 2. Optimization algorithm for light manipulation

52 Figure 1 is the schematic of the system. The Si nanolens (SiNL) is made of a nanodisk (100 nm
53 in thickness and 100 nm in radius) on a glass substrate. Its surrounding area is covered by a 40
54 nm Al film which blocks the unwanted light. Considering that it is difficult to obtain an ideal
55 perpendicular wall in fabrication, the sidewall of the nanodisk is set at 10 degree from the
56 normal direction of the substrate. Here, the wavelength of light is set at 405 nm, which is widely
57 used in lithography and fluorescence imaging.

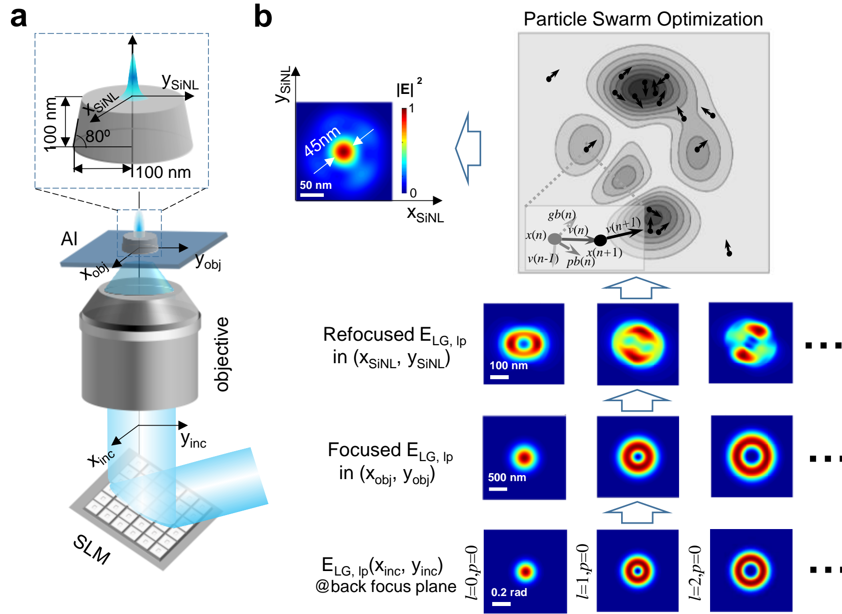

58

59 Figure 1. Simulated nanofocusing by a flat Si nanodisk lens. **a**. Schematic drawing of the model
60 system, in which spatially modulated light is focused by the objective lens and Si nanodisk
61 subsequentially. With optimization algorithm and numerical simulations, the minimum focus
62 spot can be obtained. **b**. Principle of the Laguerre-Gaussian beam-based optimization process.
63 First, focused LG beams are generated by an oil-immersion objective with spatially modulated
64 beams as shown in the bottom panels in **b**. Then, the focused beams are further focused by the
65 Si nanolens in the (x_{SiNL}, y_{SiNL}) plane. Finally, nano-focused spot is created in the (x_{SiNL}, y_{SiNL})
66 plane by linearly superposing the refocused LG beams with the help of PSO algorithm.

67

68 To focus light and further generate super-resolution patterns, spatially modulated beams
69 generated by a spatial light modulator (SLM) are used as the incident light, which are first
70 focused by an objective lens (NA = 1.4) and then further confined by the SiNL (Figure 1a).
71 As a linear optical system, the focused field by the SiNL, $\mathbf{E}_{SiNL}$, can be written as

72 $$\mathbf{E}_{SiNL} = \mathbf{M}_{SiNL}\mathbf{M}_{obj}\mathbf{E}_{in} , \quad (1)$$

73 Here, $\mathbf{E}_{in}$ are the incident fields. $\mathbf{M}_{obj}$ and $\mathbf{M}_{SiNL}$ are the optical transfer matrices of objective
74 lens and Si nanolens, respectively. To calculate the fields, we discretize the focus and back
75 focus planes of the objective into subwavelength meshes with N mesh points $\mathbf{r}_i$, $i \in [1, N]$.[32]
76 Fields $\mathbf{E}_{SiNL}$ and $\mathbf{E}_{in}$ can then be written as 3N-supervectors, $\mathbf{E}_{SiNL} = (\mathbf{E}_{SiNL}(\mathbf{r}_1), \mathbf{E}_{SiNL}(\mathbf{r}_2),...,$

77 $\mathbf{E}_{SiNL}(\mathbf{r_N}))$ and $\mathbf{E}_{in} = (\mathbf{E}_{in}(\mathbf{r_1}), \mathbf{E}_{in}(\mathbf{r_2}), ..., \mathbf{E}_{in}(\mathbf{r_N}))$; $\mathbf{M}_{obj}$ and $\mathbf{M}_{SiNL}$ becomes $3N \times 3N$ matrices.
78 Equation 1 can then be written as:

79
$$\mathbf{E}_{SiNL}(\mathbf{r}_i) = \sum_k \sum_j M_{SiNL}(\mathbf{r}_i, \mathbf{r}_k) M_{obj}(\mathbf{r}_k, \mathbf{r}_j) \mathbf{E}_{in}(\mathbf{r}_j) , \quad (2)$$

80 where, $M_{obj}(\mathbf{r}_k, \mathbf{r}_j)$ and $M_{SiNL}(\mathbf{r}_i, \mathbf{r}_k)$ are the matrices elements in $\mathbf{M}_{obj}$ and $\mathbf{M}_{SiNL}$.
81 The goal of this work is to find the incident fields $\mathbf{E}_{in}$ for a given super-resolution field
82 distribution $\mathbf{E}_{SiNL}$. To simplify this inverse problem, we write $\mathbf{E}_{in}$ into the coherent
83 superimposition of LG beams

84
$$\mathbf{E}_{in} = \sum_{lp} C_{lp} \mathbf{E}_{LG,lp} , \quad (3)$$

85 where C_{lp} are the complex coefficients, and $\mathbf{E}_{LG,lp}$ are the complex electric field distributions of
86 LG beams. Substitute $\mathbf{E}_{LG,lp}$ in Eq. (1) with Eq. (3), we have

87
$$\mathbf{E}_{SiNL} = \sum_{lp} C_{lp} \mathbf{E}_{SiNL,lp} , \quad (4)$$

88 Here, $\mathbf{E}_{SiNL,lp} = \mathbf{M}_{SiNL} \mathbf{M}_{obj} \mathbf{E}_{LG,lp}$, which presents the field distributions of the focused LG beams
89 by the SiNL.
90 Comparing to Eq. (1), Eq. (4) simplifies the problem significantly. Ideally, we only need to
91 solve coefficient C_{lp} for a given target field $\mathbf{E}_{SiNL}$. However, in the most cases, Eq. (4) is over
92 determined, and does not have a solution. In fact, we even do not know what the best achievable
93 spatial resolution for the SiNL is. To circumvent this issue, in this work, we first search for the
94 narrowest synthesized focus spots at different positions by the LG beams, and then use these
95 "points" as fundamental building blocks to construct more complex super-resolution patterns.
96 By using this method, the inverse problem becomes an optimization problem, which can be
97 solved using various algorithms. In this work, the PSO method, a global optimization algorithm,
98 was used to search for the narrowest field distributions.
99 Figure 1b shows the detailed optimization process. LG beams, $\mathbf{E}_{LG,lp}$ with l and p ranging
100 from 0 to 9 and -9 to 9 and polarization along both x and y directions were used as the incidents.
101 The corresponding focused fields $\mathbf{M}_{obj}\mathbf{E}_{LG,lp}$ at 405 nm by the objective and subsequentially
102 $\mathbf{E}_{SiNL,lp}$ by the SiNL were calculated using the Kirchhoff angular spectrum diffraction method
103 [38] and the finite-difference time-domain (FDTD) method (Lumerical FDTD), respectively
104 [39].
105 The focusing field $\mathbf{E}_{obj}(\mathbf{r})$ at the object plane can be obtained from the $\mathbf{E}_{LG,lp}$ by Kirchhoff
106 angular spectrum diffraction method [38]

107
$$\mathbf{E}_{obj}(\mathbf{r}) = \frac{ife^{-ikf}}{2\pi} \iint_{k_x,k_y} \mathbf{E}_{LG,lp}(k_x,k_y) e^{i(k_x x + k_y y + k_z z)} \frac{1}{k_z} dk_x dk_y , \quad (5)$$

108 where k_x, k_y, k_z are the components of wave vector, $k = 2\pi n_{\text{obj}}/\lambda$ is the wave number, and f is
109 the focal length of the objective lens.
110 We used the focused fields as the source in FDTD to illuminate the SiNL and calculated the
111 field distributions in the optical near-filed. Perfect matched layer boundary conditions were
112 used to eliminate unwanted reflections at the boundaries; the size of the simulated area was
113 5μm×5μm×1μm; the mesh size was 2 nm. Here, the refractive index of Si from Palik's results
114 ($n = 5.425 + i0.331$) was used in the simulation [25, 26]. With the help of $\mathbf{E}_{SiNL,lp}$, we can then
115 calculate the corresponding coefficients C_{lp} in Eq. 4 for given target field distributions with
116 the PSO algorithm.
117 In the PSO calculations, multiple parameters are considered in the optimization process to
118 obtain a meaningful super-resolution focus with a clean background, symmetric shape and large
119 focus depth. More detailed, we defined a certain number of particles in a high-dimensional
120 parameter space spanned by C_{lp}, the coefficients in Eq. (4). The particles moved in this
121 parameter space via a stochastic optimization process to find the optimal value of a pre-defined

122 merit function [35, 36]. Here, the merit function includes all the key parameters for the
123 nanofocusing process, namely the size, depth and position of the focus spots. We iterated 5000
124 times with a swarm of 60 particles in each calculation and we repeated this process until
125 satisfactory results were found. Linear decreasing weight and contraction factor were used to
126 accelerate the convergence rate and obtain high quality solutions. The detailed optimization
127 strategy is discussed in the later section of this work.

128 **3. Sub-50 nm focus of light**

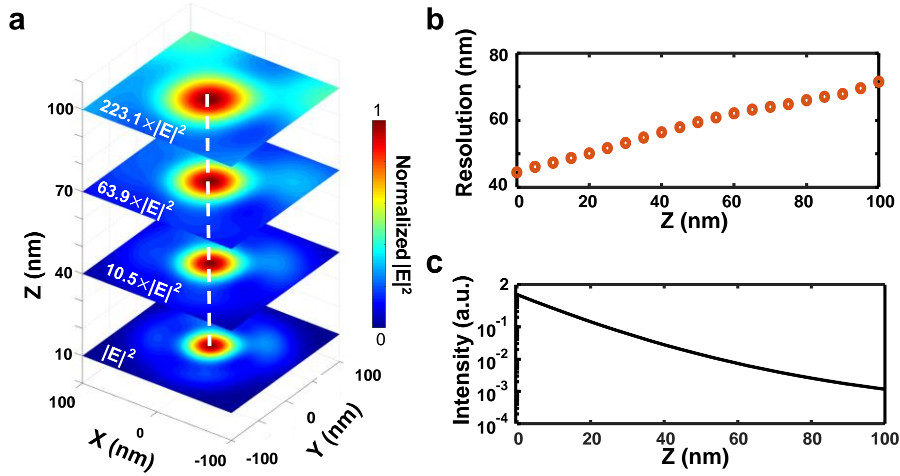

129

130 Fig. 2. Nanofocusing behavior of the Si nanolens at different height, z. a. Field distribution at z
131 = 10, 40, 70 and 100 nm. b. Size of the focus spot as a function of z. c. Height-dependent peak
132 intensity of the nano-focused fields.

133 Using the above method, we first searched for the simplest case of super-resolution light
134 modulation, namely the nano-focus at the center point of the SiNL by setting the target position
135 at (0, 0) in the PSO algorithm. Figure 1b shows the result. A symmetric nano-focus spot was
136 obtained without any strong sidelobes. The full width of half maximum (FWHM) reaches 45
137 nm at $z = 0$ nm, which is smaller than $\lambda/9$ and much smaller than diffraction limit ($\lambda/2NA$).
138 In addition to the extreme lateral confinement, the depth of the nano-focus spot reaches
139 almost 100 nm in air. We plot the field distribution at different heights (10 nm, 40 nm, 70 nm
140 and 100 nm), as shown in figure 2a. The size of the nano-focus spot increases slowly along the
141 z direction. At $z = 100$ nm, the spot size is still smaller than 100 nm. It is worth noting that
142 although the lateral confinement of nano-focus spot is kept, the intensity of focus spot drops
143 exponentially along the z direction (Fig. 2c). It indicates that the nano-focusing effect is
144 essentially a near-field effect.

145 **4. Nano-focusing at any given position**

146 After achieving nano-focusing at the center of the SiNL, a natural question is whether we can
147 synthesize such a nano-spot at other positions. To answer this question, we changed the target
148 position in the merit function and ran the optimization algorithm for each point. Since the SiNL
149 is an axial symmetric structure, we only need to consider the focus behaviors along its radius
150 (e.g., the x-axis in this work). If nano-focusing can be achieved at any position along the x-axis,
151 we then will be able to focus light at a given position in the whole plane by simply rotating the
152 system as shown in figure 3a.
153 Here, we set a series of target positions of the nano-focus spots along the x-axis with a 10
154 nm step (i.e., x_{foc} = 10 nm, 20 nm, 30 nm, 40 nm, 50 nm and 60 nm). Figure 3b shows the
155 optimized results. Light can be tightly focused into a nano-spot (FWHM < 60 nm) at all the 6

156 positions with intensity of the sidelobes kept below half of the intensity of the main focus spot.
157 In addition, the depths of all the nano-focus spots exceed 100 nm are similar to the case of the
158 focus spot at (0, 0).

159 The above results show that the field of view (FOV) of the SiNL can reach 120 nm (a
160 circular area with radius of 60 nm). Within the FOV, light can always be focused into a deep
161 subwavelength nano-spot with a depth of focus (DOF) over several tens of nanometers (Fig. 3c
162 and 3d). In other words, the spot size is kept below 100 nm within the DOF. We also test the
163 cases with $x_{foc} > 60$ nm. Focus spots can still be obtained, but their shapes become asymmetric
164 and the sizes are considerable larger than 50 nm.
165

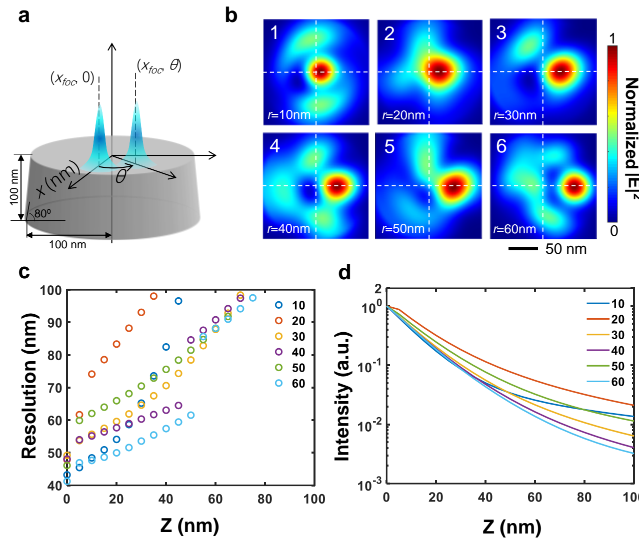

166

167 Fig. 3. Nanofocus at different positions of the Si nanolens. a. Focus spot at (x_{foc}, θ) can be
168 obtained by rotating an optimized nano-focus spot (x_{foc}, 0) on x-axis. b. Synthesized nano-
169 focusing spots at different positions on x-axis (x = 10, 20, 30, 40, 50 and 60 nm). c. Size of the
170 focus spot as a function of z at different positions. d. Height-dependent peak intensity of the
171 nano-focused fields at different positions.

172

173 ## 5. Super-resolution spatial light modulation

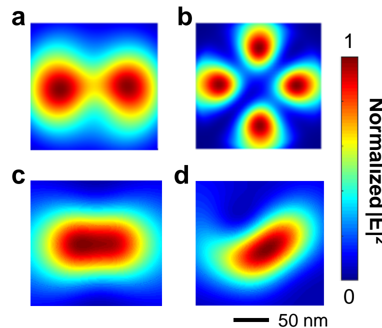

174

175 Fig. 4. Nanopattern generation by the Si nanolens. a and b. Synthesized point pair and 2-by-2
176 point arrays. c and d. Synthesized super-resolution lines along the x-axis and diagnostics.

Once we can obtain nano-focus spots at any given position in the FOV, we can generate any super-resolution patterns by using the linear superposition of several different nano-spots. To demonstrate this capacity, we here tested two different types of patterns, point arrays and lines.

As shown in Fig. 4a and 4b, two different point array patterns are synthesized, namely point pair and 2-by-2 array. The patterns are composted of focused point 60 nm away from the center point of the FOV. After the supposition, all the spots are still well separated. In the process, the size of the each spot slightly increases due to the background induced by the rest nano-focus spots. Here, a further step of optimization was implemented based on the supposition results to further rectify the shape and suppress the undesired background.

In addition to the point array, super-resolution lines can also be constructed by the SiNL. Here, we take lines along the *x*-axis and diagnostics as examples. As shown in Figure 4c and 4d, the lengths of the lines exceed 100 nm, and the width is below 60 nm. Similar to the case of point arrays, an additional step of optimization was used to perfect the shapes of the lines.

6. Multi-step optimization strategy

To achieve above demonstrated super-resolution patterns, the key is to choose a proper optimization strategy. Particularly, in this work, multiple independent parameters are required to quantify the quality of a single nano-focus spot (namely, position, size, symmetry, size of sidelobes and depth of focus). It makes the choice of the detailed optimization process, as well as the merit function, a challenging task. For example, if all the parameters are considered in the same time, we will not be able to find satisfactory results in the most case. By setting optimization strategy as merit function, the optimization process of PSO can be constrained. For example, if the center region is set as the range of the strongest point of light intensity, the results of the non-strongest point of the center can be discarded. This method reduces the computation and saves the convergence time. Based on the above consideration, here, we use a multi-step optimization strategy, in which the lateral profile and DOF of the focused fields are considered separately in subsequent steps.

One of the major challenges in the lateral optimization process is how to quantitively evaluate the shape and size of the focused spots, which can be in any irregular shapes. Here, the isoline at 50% of the maximum intensity is used to describe the shape of focus spot. More detailed, we use the radius of the smallest excircle of the 50% isoline, R_{max}, as the spot size, and define $\eta = R_{min}/R_{max}$, the ratio between radius of the smallest excircle and largest incircle of the 50% isoline to evaluate the symmetry of the spot.

After the optimal lateral profiles (i.e., focus spots with the smallest R_{max} and η) are found at the z = 20 nm plane, we further optimize the DOF of the focus spots to avoid the cases of extremely small DOF. More detailed, we use $\sum_i z_i R_{max,i}$, the sum of the product between height z_i (ranging from 10 nm to 200 nm) and lateral size $R_{max,i}$ at z_i as the merit function to search for the best results. This will finally lead to the nano-focus spot with a large DOF.

7. Role of polarization in nano-focusing

In addition to the optimization strategy, the polarization of LG beams can also influence the quality of the nano-focuses. It requires both LG beams with *x*-polarization and *y*-polarization to achieve a nano-focus spot below 45 nm. When only *x*-polarized LG beams are used, the optimized results are considerably larger (always > 55 nm), as shown in Figure 5. Moreover, the relative intensity of the sidelobes also becomes larger (reaches 0.7) and the DOF becomes smaller than 50nm.

In order to understand the behind mechanism, we plotted the polarization of the electric fields at different height, as shown in Figure 5a and 5b. In the case that both *x*- and *y*-polarized LG beam are used, there are two vortices formed in the close vicinity of the central axis of the SiNL, and these two vortices form low intensity areas which pinch the fields into a tightly focused spot along the central axis. More importantly, due to the vortices, the structure of the

227 focused fields stay unchanged along *z*, and this leads to the large DOF. On the contrary, there
228 is not such parallel vortices in the case of focused field synthesized by only *x*-polarized LG-
229 beams. As a result, the structure of electric fields varies along *z*-axis, and the focus spot diverges
230 rapidly, as shown in Figure 5b. It worth noting that the coexistence of vortices and field
231 localization is a common phenomenon, which has been found in other types of super-resolution
232 focus spots [40].

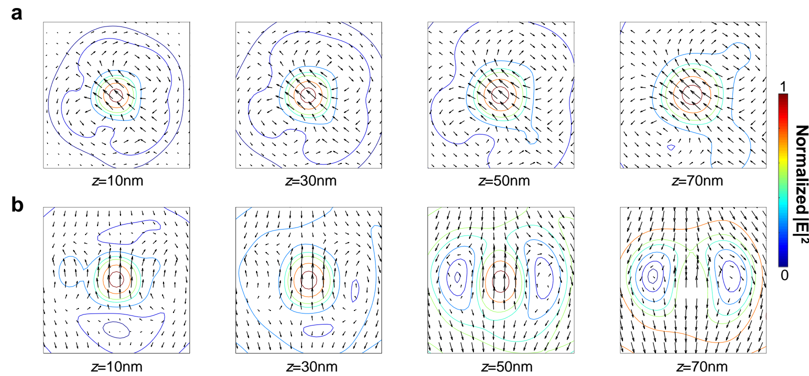

233

234 Fig. 5. Polarization effect in nano-focusing. a. Polarization maps of the nano-focusing spot by
235 both *x*- and *y*-polarized LG beams at different *z*. The contour maps are shows the intensity
236 distribution. b. Polarization maps of the nano-focusing spot *x*-polarized LG beams.

237

238 8. Size effect of the SiNL

239 Finally, we would like to emphasize that the performance of the SiNL is not sensitive to its size.
240 When the thickness of SiNL is comparable to or less than the penetration depth of the Si (195
241 nm at 405 nm) and the radius is comparable to the thickness, we can always achieve a nano-
242 focus spot approximately 50 nm. More detailed, we tested SiNL with R ranging from 50 nm to
243 250 nm, and thickness from 100 nm to 200 nm. The size of the optimized focus spot is always
244 below 60 nm, and no correlation between the size of nano-focus spots and size of SiNL is found.
245 It means that SiNLs are able to tolerate shape discrepancies induced in fabrication processes.

246 9. Summary

247 In summary, we studied the super-resolution light modulation capability of a flat Si nanolens
248 at 405 nm, which is semi-transparent and has a refractive index > 5. A Laguerre-Gaussian beam
249 expansion-based optimization method was established to synthesize nano-focus spots on the
250 upper-surface of the SiNL. With this method, we realized a nano-focus at the center of the
251 nanolens with a FWHM of 45 nm and DOF larger than 100nm. Moreover, we can obtain such
252 a nano-focus spot at any positions in the whole center area of the nanolens (120 nm in diameter)
253 and further utilize these nano-spots as building blocks for constructing more complex super-
254 resolution patterns, including point arrays and lines by linearly combining several separated
255 nano-focus spots together. Finally, we investigated the nano-focusing capability of Si nanolens
256 with different sizes, and found that their performance is not sensitive to the geometrical
257 parameters. We believe that this flat Si nanodisk lenses, with its superb nano-focusing
258 capability and fabrication-friendly design, can have important applications in super-resolution
259 imaging and lithography.

260 Funding

261 This study was supported by grants from the National Key Technologies R&D Program of
262 China (No. 2016YFA0201104).

263 **Disclosures.**

264 The authors declare no conflicts of interest.

265

266 References

267

268 1. H. Kawata, J. M. Carter, A. Yen, and H. I. Smith, "Optical projection lithography using lenses with numerical
269 apertures greater than unity," Microelectronic Engineering **9**, 31-36 (1989).
270 2. G. J. Brakenhoff, P. Blom, and P. Barends, "Confocal scanning light-microscopy with high aperture immersion
271 lenses," Journal of Microscopy-Oxford **117**, 219-232 (1979).
272 3. H. E. Keller, "Objective Lenses for Confocal Microscopy," in *Handbook Of Biological Confocal Microscopy*, J.
273 B. Pawley, ed. (Springer US, Boston, MA, 2006), pp. 145-161.
274 4. T. Ito and S. J. N. Okazaki, "Pushing the limits of lithography," Nature **406**, 1027-1031 (2000).
275 5. A. Raub and S. Brueck, *Deep UV immersion interferometric lithography*, Microlithography 2003 (SPIE, 2003),
276 Vol. 5040.
277 6. M. Totzeck, W. Ulrich, A. Göhnermeier, and W. Kaiser, "Pushing deep ultraviolet lithography to its limits,"
278 Nat. Photon. **1**, 629-631 (2007).
279 7. J. Y. Lee, B. H. Hong, W. Y. Kim, S. K. Min, Y. Kim, M. V. Jouravlev, R. Bose, K. S. Kim, I. C. Hwang, L. J.
280 Kaufman, C. W. Wong, P. Kim, and K. S. Kim, "Near-field focusing and magnification through self-assembled
281 nanoscale spherical lenses," Nature **460**, 498-501 (2009).
282 8. Z. Wang, W. Guo, L. Li, B. Luk'yanchuk, A. Khan, Z. Liu, Z. Chen, and M. Hong, "Optical virtual imaging at
283 50 nm lateral resolution with a white-light nanoscope," Nat. Commun. **2**, 218 (2011).
284 9. W. Fan, B. Yan, Z. B. Wang, and L. M. Wu, "Three-dimensional all-dielectric metamaterial solid immersion
285 lens for subwavelength imaging at visible frequencies," Sci. Adv. **2**, e1600901 (2016).
286 10. A. Darafsheh, G. F. Walsh, L. Dal Negro, and V. N. Astratov, "Optical super-resolution by high-index liquid-
287 immersed microspheres," Appl. Phys. Lett. **101**, 141128 (2012).
288 11. H. Yang, N. Moullan, J. Auwerx, and M. A. M. Gijs, "Super-Resolution Biological Microscopy Using Virtual
289 Imaging by a Microsphere Nanoscope," Small **10**, 1712-1718 (2014).
290 12. F. Wang, L. Liu, H. Yu, Y. Wen, P. Yu, Z. Liu, Y. Wang, and W. J. Li, "Scanning superlens microscopy for
291 non-invasive large field-of-view visible light nanoscale imaging," Nat. Commun. **7**, 13748 (2016).
292 13. F. G. Wang, S. L. Yang, H. F. Ma, P. Shen, N. Wei, M. Wang, Y. Xia, Y. Deng, and Y. H. Ye, "Microsphere-
293 assisted super-resolution imaging with enlarged numerical aperture by semi-immersion," Appl. Phys. Lett. **112**,
294 023101 (2018).
295 14. N. Franch, J. Canals, V. Moro, A. Vila, A. Romano-Rodriguez, J. D. Prades, J. Gulink, D. Bezshlyakh, A.
296 Waag, K. Kluczyk-Korch, M. Auf der Maur, A. di Carlo, and A. Dieguez, "Nano illumination microscopy: a
297 technique based on scanning with an array of individually addressable nanoLEDs," Opt. Express **28**, 19044-
298 19057 (2020).
299 15. J. Haug, M. Palei, J. D. Shrout, E. Narimanov, P. W. Bohn, and A. J. Hoffman, "Confined hyperbolic
300 metasurface modes for structured illumination microscopy," Opt. Express **29**, 42331-42342 (2021).
301 16. K. Koyama, M. Yoshita, M. Baba, T. Suemoto, and H. Akiyama, "High collection efficiency in fluorescence
302 microscopy with a solid immersion lens," Appl. Phys. Lett. **75**, 1667-1669 (1999).
303 17. Z. H. Liu, B. B. Goldberg, S. B. Ippolito, A. N. Vamivakas, M. S. Unlu, and R. Mirin, "High resolution, high
304 collection efficiency in numerical aperture increasing lens microscopy of individual quantum dots," Appl. Phys.
305 Lett. **87**, 071905 (2005).
306 18. D. Wildanger, B. R. Patton, H. Schill, L. Marseglia, J. P. Hadden, S. Knauer, A. Schoenle, J. G. Rarity, J. L.
307 O'Brien, S. W. Hell, and J. M. Smith, "Solid Immersion Facilitates Fluorescence Microscopy with Nanometer
308 Resolution and Sub-Angstrom Emitter Localization," Adv. Mater. **24**, OP309-OP313 (2012).
309 19. L. Liang, D. B. L. Teh, N.-D. Dinh, W. Chen, Q. Chen, Y. Wu, S. Chowdhury, A. Yamanaka, T. C. Sum, C.-H.
310 Chen, N. V. Thakor, A. H. All, and X. Liu, "Upconversion amplification through dielectric superlensing
311 modulation," Nat. Commun. **10**, 1391 (2019).
312 20. L. P. Ghislain, V. B. Elings, K. B. Crozier, S. R. Manalis, S. C. Minne, K. Wilder, G. S. Kino, and C. F. Quate,
313 "Near-field photolithography with a solid immersion lens," Appl. Phys. Lett. **74**, 501-503 (1999).
314 21. M. M. Alkaisi, R. J. Blaikie, S. J. McNab, R. Cheung, and D. R. S. Cumming, "Sub-diffraction-limited
315 patterning using evanescent near-field optical lithography," Appl. Phys. Lett. **75**, 3560-3562 (1999).
316 22. M. C. Gwinner, E. Koroknay, L. Fu, P. Patoka, W. Kandulski, M. Giersig, and H. Giessen, "Periodic large-area
317 metallic split-ring resonator metamaterial fabrication based on shadow nanosphere lithography," Small **5**, 400-
318 406 (2009).
319 23. D. E. Aspnes and A. A. Studna, "Dielectric Functions and Optical-Parameters of Si, Ge, Gap, Gaas, Gasb, Inp,
320 Inas, and Insb from 1.5 to 6.0 Ev," Phys. Rev. B **27**, 985-1009 (1983).
321 24. H. Ehrenreich and F. Spaepen, *Solid state physics* (Academic Press, New York, 2001), Vol. 56.
322 25. E. D, "Silicon (Si)," in *Handbook of Optical Constants of Solids*, E. D. Palik, ed. (Academic Press, New York,
323 1998).

324 26. Z. Wang and W. Zhang, "Sub-50 nm focusing of a 405 nm laser by hemispherical silicon nanolens," J. Opt.
325 Soc. Am. B **38**, 44-50 (2020).
326 27. K. Huang, H. P. Ye, J. H. Teng, S. P. Yeo, B. Luk'yanchuk, and C. W. Qiu, "Optimization-free superoscillatory
327 lens using phase and amplitude masks," Laser Photon. Rev. **8**, 152-157 (2014).
328 28. I. Malkiel, M. Mrejen, A. Nagler, U. Arieli, L. Wolf, and H. Suchowski, "Plasmonic nanostructure design and
329 characterization via Deep Learning," Light Sci. Appl. **7**, 60 (2018).
330 29. H. Ren, W. Shao, Y. Li, F. Salim, and M. Gu, "Three-dimensional vectorial holography based on machine
331 learning inverse design," Sci. Adv. **6**, 4261 (2020).
332 30. M. Bancerek, K. M. Czajkowski, and R. Kotynski, "Far-field signature of sub-wavelength microscopic objects,"
333 Opt. Express **28**, 36206-36218 (2020).
334 31. L. H. Yeh, L. Tian, and L. Waller, "Structured illumination microscopy with unknown patterns and a statistical
335 prior," Biomed Opt Express **8**, 695-711 (2017).
336 32. G. Volpe, G. Molina-Terriza, and R. Quidant, "Deterministic Subwavelength Control of Light Confinement in
337 Nanostructures," Phys. Rev.Lett. **105**, 216802 (2010).
338 33. L. Allen, M. W. Beijersbergen, R. J. Spreeuw, and J. P. Woerdman, "Orbital angular momentum of light and the
339 transformation of Laguerre-Gaussian laser modes," Phys. Rev. A **45**, 8185-8189 (1992).
340 34. C. Rosales-Guzman, B. Ndagano, and A. Forbes, "A review of complex vector light fields and their
341 applications," J. Opt. **20**, 123001 (2018).
342 35. Y. J. Shen, X. J. Wang, Z. W. Xie, C. J. Min, X. Fu, Q. Liu, M. L. Gong, and X. C. Yuan, "Optical vortices 30
343 years on: OAM manipulation from topological charge to multiple singularities," Light Sci. Appl. **8**, 90 (2019).
344 36. J. Robinson and Y. Rahmat-Samii, "Particle Swarm Optimization in Electromagnetics," IEEE Trans. Antennas
345 Propag. **52**, 397-407 (2004).
346 37. E. T. Rogers, J. Lindberg, T. Roy, S. Savo, J. E. Chad, M. R. Dennis, and N. I. Zheludev, "A super-oscillatory
347 lens optical microscope for subwavelength imaging," Nat. Mater. **11**, 432-435 (2012).
348 38. L. Novotny and H. B, *Principles of Nano-Optics* (Cambridge University Press, New York, 2006).
349 39. A. Taflove and S. C. Hagness, *Computational electrodynamics: the finite-difference time-domain method*
350 (Artech house, 2005).
351 40. G. Yuan, E. T. F. Rogers, and N. I. Zheludev, "“Plasmonics” in free space: observation of giant wavevectors,
352 vortices, and energy backflow in superoscillatory optical fields," Light Sci. Appl. **8**, 2 (2019).

353

View publication stats